High-rate electrochemical energy storage through Li+ intercalation pseudocapacitance

Veronica Augustyn, Jérémy Come, Michael A. Lowe, Jong Woung Kim, Pierre-Louis Taberna, Sarah H. Tolbert, Héctor D. Abruña, Patrice Simon, Bruce Dunn

High-rate electrochemical energy storage through Li^+ intercalation pseudocapacitance

Veronica Augustyn[1], Jérémy Come[2,3], Michael A. Lowe[4], Jong Woung Kim[1], Pierre-Louis Taberna[2,3], Sarah H. Tolbert[5], Héctor D. Abruña[4], Patrice Simon[2,3] and Bruce Dunn[1]*

Pseudocapacitance is commonly associated with surface or near-surface reversible redox reactions, as observed with $RuO_2 \cdot xH_2O$ in an acidic electrolyte. However, we recently demonstrated that a pseudocapacitive mechanism occurs when lithium ions are inserted into mesoporous and nanocrystal films of orthorhombic Nb_2O_5 (*T*-Nb_2O_5; refs 1,2). Here, we quantify the kinetics of charge storage in *T*-Nb_2O_5: currents that vary inversely with time, charge-storage capacity that is mostly independent of rate, and redox peaks that exhibit small voltage offsets even at high rates. We also define the structural characteristics necessary for this process, termed intercalation pseudocapacitance, which are a crystalline network that offers two-dimensional transport pathways and little structural change on intercalation. The principal benefit realized from intercalation pseudocapacitance is that high levels of charge storage are achieved within short periods of time because there are no limitations from solid-state diffusion. Thick electrodes (up to 40 μm thick) prepared with *T*-Nb_2O_5 offer the promise of exploiting intercalation pseudocapacitance to obtain high-rate charge-storage devices.

Pseudocapacitance occurs whenever the charge (Q) depends on the change in potential (dE), yielding a capacitance (dQ/dE) (ref. 3). The capacity can be due to monolayer adsorption of ions at an electrode surface, as in the underpotential deposition of metals[4]; surface redox reactions as in RuO_2; or ion intercalation that does not result in a phase change. Although these redox processes are Faradaic in nature, their phenomenological behaviour, and response to experimental variables such as sweep rate, are those typical of capacitors. All of these scenarios produce a relationship between the fractional extent of charge storage, X, and the potential of the form[3,5]:

$$E \sim \left(\frac{RT}{nF}\right) \ln\left[\frac{X}{(1-X)}\right] \qquad (1)$$

where R is the ideal gas constant (J mol^{-1} K^{-1}), T is the temperature (K), F is Faraday's constant (96,485 As mol^{-1}) and n is the number of electrons involved in the reaction. In all of these cases, a constant-current experiment yields a potential E that changes with the extent of charge Q according to:

$$Q = C\Delta E$$

where Q is the charge passed (Coulombs), ΔE is the potential change (V) and C is the pseudocapacitance (F). This behaviour is typical of capacitive charge/discharge, thus leading to the term pseudocapacitance[3].

Of the three pseudocapacitive mechanisms mentioned above, underpotential deposition and surface redox reaction pseudocapacitance exhibit kinetics indicative of surface-controlled electrochemical processes[6]:

$$i = Cv$$

where i is the current (A) and v is the sweep rate (mV s^{-1}) of a cyclic voltammetry experiment. However, in intercalation pseudocapacitance, as described herein, charge storage does not occur on the surface but in the bulk material. The kinetics are not diffusion-limited and instead are limited by surface processes so that the overall behaviour seems capacitive. Intercalation pseudocapacitance is rarely observed because in most intercalation materials charge storage (even in thin films, as in anatase TiO_2; refs 7,8) is limited by solid-state diffusion and therefore the peak currents scale with $v^{1/2}$.

Here we investigate the phenomenon of intercalation pseudocapacitance and the high-rate behaviour of *T*-Nb_2O_5 using two different electrode techniques that provide a wide variation in sweep rates. For timescales between ~3 h and 60 s (sweep rates of 0.1–20 mV s^{-1} within a voltage window of 1.2 V), we used a thin-film electrode. For shorter timescales where ohmic polarization is significant (60–500 mV s^{-1}), we used a cavity microelectrode where the active material was mixed with a conductive carbon black to alleviate the loss of electrical transport (ohmic losses)[9]. To confirm the small ohmic drop of this electrode, we performed cyclic voltammetry from 100–500 mV s^{-1} in a bulky-ion electrolyte (Supplementary Fig. S1). In addition, we prepared thick films (~40 μm) of *T*-Nb_2O_5 to determine whether the high-rate capability was limited to thin films.

Charge storage from the intercalation of lithium ions into Nb_2O_5 can be expressed as:

$$Nb_2O_5 + xLi^+ + xe^- \leftrightarrow Li_xNb_2O_5$$

where the maximum capacity is $x = 2$ (ref. 10). Figure 1a shows cyclic voltammograms from 100 to 500 mV s^{-1} in a cavity microelectrode where it is evident that both anodic and cathodic peaks are broad, about 600 mV. There is also a noticeable peak shift (and increase in peak separation ΔE_p) as the sweep rate increases, but the capacity remains reversible. Figure 1b presents a plot of $\log(i)$ versus $\log(v)$ from 0.1 to 500 mV s^{-1} for both cathodic and anodic peaks. Assuming that the current obeys a power-law

[1]Department of Materials Science and Engineering, University of California, Los Angeles, California 90095, USA, [2]Department of Materials Science, Université Paul Sabatier, CIRIMAT UMR CNRS 5085, Toulouse 31062, France, [3]Réseau sur le Stockage Electrochimique de l'Energie (RS2E), FR CNRS 3459, France, [4]Department of Chemistry and Chemical Biology, Cornell University, Ithaca, New York 14853, USA, [5]Department of Chemistry and Biochemistry, University of California, Los Angeles, California 90095, USA. *e-mail: bdunn@ucla.edu.

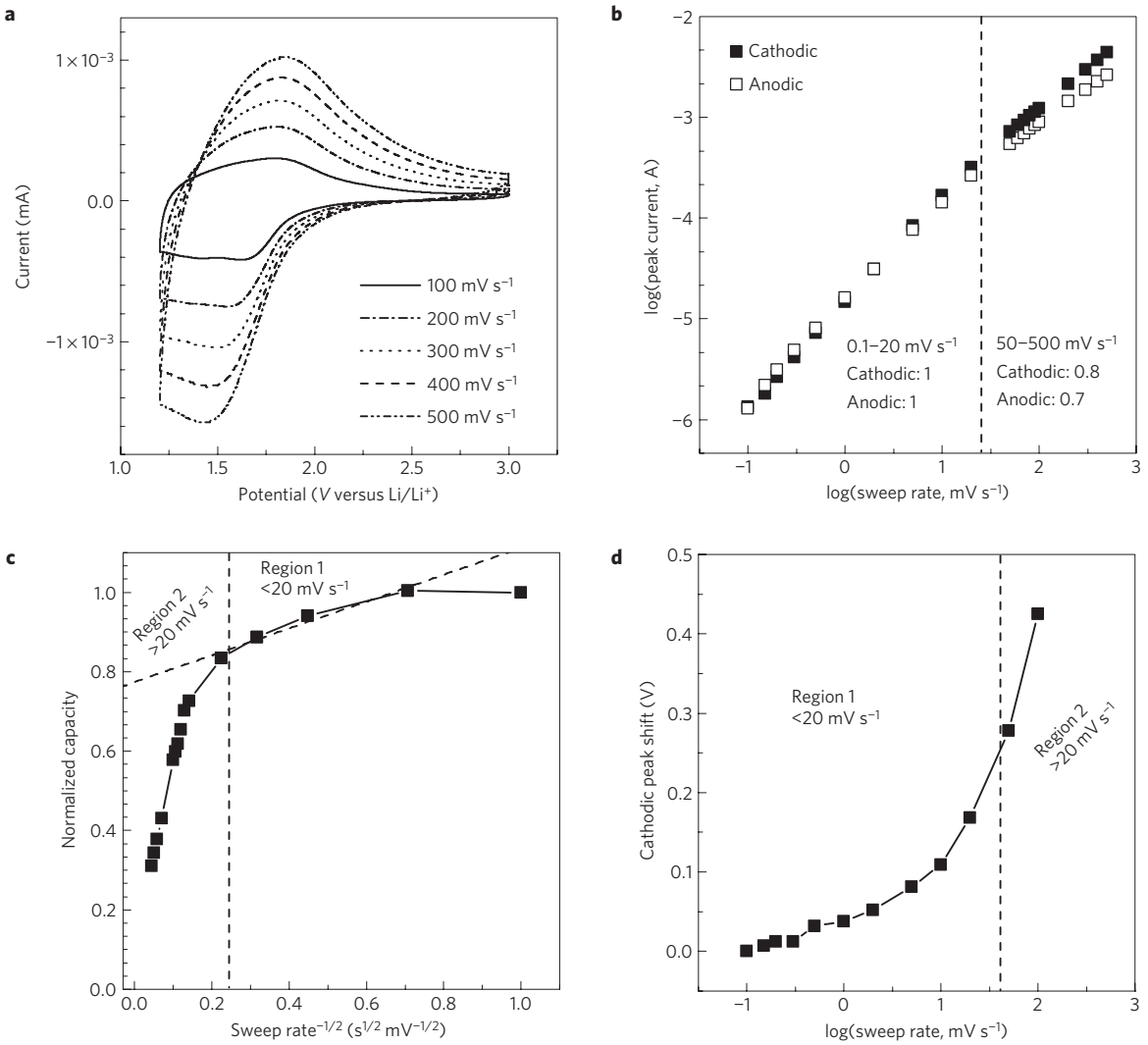

Figure 1 | Kinetic analysis of the electrochemical behaviour of *T*-Nb_2O_5. a, Cyclic voltammograms from 100 to 500 mV s^{-1} demonstrate the high-rate capability of the material. **b**, *b*-value determination of the peak anodic and cathodic currents shows that this value is approximately 1 up to 50 mV s^{-1}. This indicates that even at the peak currents, charge storage is capacitive. **c**, Capacity versus $v^{-1/2}$ allows for the separation of diffusion-controlled capacity from capacitive-controlled capacity; two distinct kinetic regions emerge when the sweep rate is varied from 1 to 500 mV s^{-1}. The dashed diagonal line corresponds to the extrapolation of the infinite sweep rate capacitance using the capacity between 2 and 20 mV s^{-1}. **d**, The variation of the cathodic peak voltage with the sweep rate exhibits a region of small peak separation followed by increased separation at 20 mV s^{-1}, and represents another method of identifying systems with facile intercalation kinetics.

relationship with the sweep rate leads to[8]:

$$i = av^b$$

where *a* and *b* are adjustable values. Whereas a *b*-value of 0.5 would indicate that the current is controlled by semi-infinite linear diffusion, a value of 1 indicates that the current is surface-controlled. For sweep rates ranging from 0.1 to 20 mV s^{-1}, corresponding to charging times >60 s, the *b*-value for both the cathodic and anodic peaks is 1, indicating that the kinetics are surface-controlled, and thus fast. Figure 1b also exhibits a change in the slope of the anodic and cathodic peak currents at ~50 mV s^{-1}. This change in slope corresponds to a decrease in *b*-value to 0.8 and 0.7 for the cathodic and anodic currents, respectively, at sweep rates >50 mV s^{-1} (charging times <20 s). This limitation to the rate capability can arise from numerous sources including an increase of the ohmic contribution (active material resistance, solid–electrolyte interphase resistance) and/or diffusion constraints/limitations[11]. In the limit of slow diffusion, *b* would approach a value of 0.5 as described above.

The relationship between capacity and sweep rate can also establish the rate-limiting step of a charge-storage mechanism[12]. In a plot of *Q* versus $v^{-1/2}$, regions that are linear represent capacity limited by semi-infinite linear diffusion whereas capacitive contributions are independent of the sweep rate. At sweep rates below 20 mV s^{-1}, the extrapolated *y*-intercept yields the infinite sweep rate capacitance[13]. Figure 1c shows the plot of normalized capacity versus $v^{-1/2}$ for *T*-Nb_2O_5 from 1 to 500 mV s^{-1} (the gravimetric capacity for the thin-film electrode is shown in Supplementary Fig. S2). Analogous to the behaviour of the peak current in Fig. 1b, there are two distinct regions in Fig. 1c. In region 1, at sweep rates <20 mV s^{-1}, the capacity is mostly independent of sweep rate. The magnitude of the capacity is ~130 mAh g^{-1} or ~65% of the theoretical value based on a two-electron redox reaction with Nb_2O_5. In this range, solid-state lithium-ion diffusion is not the rate-limiting step for charge storage. In region 2, from 50 to 500 mV s^{-1}, the capacity decreases linearly with $v^{-1/2}$. This indicates that charge storage is mainly diffusion-controlled at high sweep rates. That is, for charging times

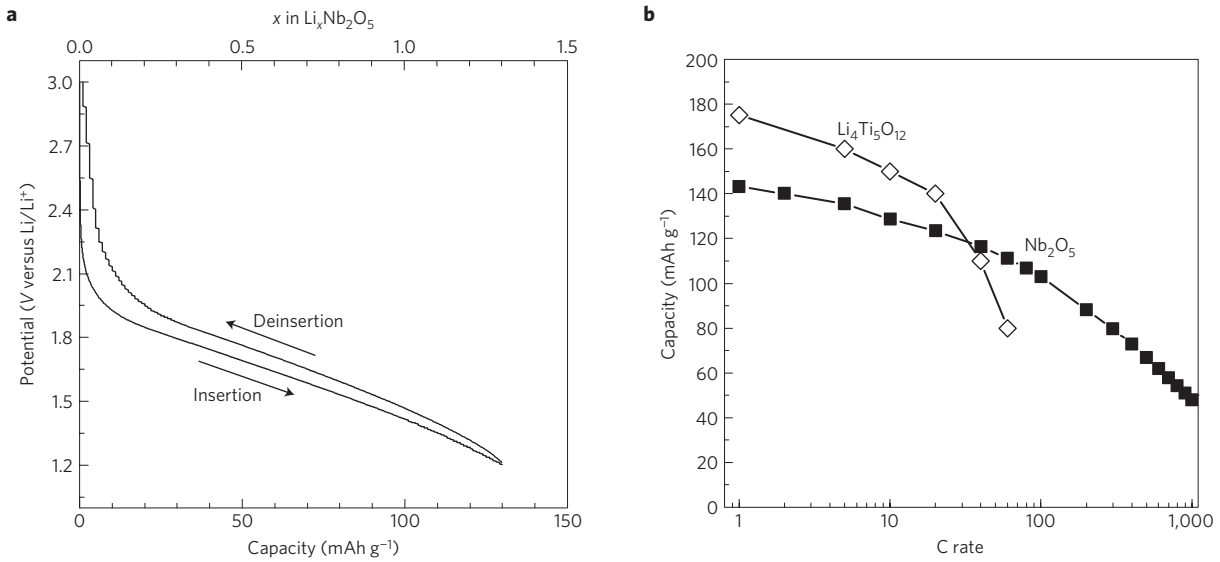

Figure 2 | Electrochemical cycling of a 40-μm-thick *T*-Nb_2O_5 electrode. a, Galvanostatic cycling of a thick Nb_2O_5 electrode at a 10C rate. **b**, Comparison of the rate capability of *T*-Nb_2O_5 with a high-rate lithium-ion anode, $Li_4Ti_5O_{12}$, at various C-rates ($Li_4Ti_5O_{12}$ data reproduced from ref. 16).

of <20 s, diffusion is rate-limiting, similar to most traditional battery electrodes. However, for charging times of 1 min (60C) or longer, there is no indication of diffusion limitations and this intercalation-based system behaves in a fully capacitive manner.

Another feature of *T*-Nb_2O_5 at sweep rates <20 mV s^{-1} is that the peak voltage shifts with sweep rate are small (Fig. 1d). The cathodic peak shift is <0.1 V at sweep rates below 10 mV s^{-1}. As a result, the anodic and cathodic peaks overlap at 0.1 mV s^{-1} (Supplementary Fig. S3) and it is in this behaviour that the similarity to surface redox reactions is most apparent[14]. In many lithium-ion intercalation materials, the peak separation is significant even in thin films and at slow sweep rates (for example, $\Delta E_p = 0.13$ V for $LiCoO_2$ at 0.1 mV s^{-1}; ref. 15). This type of behaviour is often associated with crystallographic phase changes during the Faradaic process, and contrasts with intercalation materials that form a solid solution, such as *T*-Nb_2O_5. Besides identifying facile intercalation, the peak voltage separation is related to the high-power capability of a material. As the charging time decreases, that is, at higher current densities, the peak separation in a battery material increases owing to polarization (reflecting the higher overpotentials necessary to deliver the higher currents), so that at higher rates the energy required to fully charge the material is significantly larger than the energy available on discharge.

The high-rate behaviour of *T*-Nb_2O_5 is not limited to thin films or to experiments with small amounts of active material. The constant-current charge/discharge of a 40-μm-thick *T*-Nb_2O_5 (1 mg cm^{-2}) electrode at a 10C rate is shown in Fig. 2a. At this rate, the capacity is 130 mAh g^{-1} and E varies linearly with Q as expected for a pseudocapacitive process from equation (1). This represents capacities typical of battery materials but at rates closer to those of supercapacitors. The rate capability of *T*-Nb_2O_5 from 1 to 1,000C is shown in Fig. 2b and compared with that of $Li_4Ti_5O_{12}$ (of comparable electrode dimensions)[16]. $Li_4Ti_5O_{12}$ is chosen as an example of a high-rate lithium-ion anode material. The rate capability for *T*-Nb_2O_5 is significantly better than $Li_4Ti_5O_{12}$ above 30C and even at a 1,000C rate the capacity of the thick *T*-Nb_2O_5 electrode is ~40 mAh g^{-1}. The thick electrode results verify that the intercalation pseudocapacitance mechanism is not due to thin-film or surface effects, such as vacancies or contributions of the first few atoms from the surface. Indeed, even for the thick electrode, the *b*-values for the anodic and cathodic peak currents are 1 from 1 to 10 mV s^{-1} (Supplementary Fig. S4).

The high-rate capability of *T*-Nb_2O_5 implies that the crystal structure permits exceptionally rapid ionic transport. As shown in Fig. 3a, the unit cell has sheets of edge- or corner-sharing distorted polyhedra lying parallel to the (001) plane, with each Nb^{5+} surrounded by either 6 or 7 O^{2-}. The polyhedra are exclusively corner-sharing along the [001] direction with 5% of the Nb^{5+} ions randomly located in 9-coordinate sites between the (001) polyhedral planes[17]. The mostly empty octahedral sites between (001) planes provide natural tunnels for lithium-ion transport throughout the *a*–*b* plane. Calculations indicate that the (001) plane allows degenerate pathways with low energy barriers for ion transport[18].

A previous *in situ* X-ray diffraction study showed that the insertion of lithium into *T*-Nb_2O_5 results in a solid solution with no apparent phase changes[19], and negligible changes to lattice constants[2] and unit-cell volume[20] up to ~1.25 Li^+/Nb_2O_5. *In situ* X-ray absorption spectroscopy (XAS) demonstrated that lithiation reduces Nb^{5+} to Nb^{4+} (ref. 19). The *in situ* XAS studies carried out here confirm that lithiation results in a continuous change in oxidation state (Fig. 3b) and the Fourier-transform of the extended X-ray absorption fine structure (EXAFS) indicates that the insertion reaction proceeds through two stages (Fig. 3c). From 2.5 to 1.75 V, the EXAFS signal from the various Nb–O bond lengths in Nb_2O_5 (1.40–1.85 Å) merges to a single peak at an intermediate bond length (1.75 Å), indicating that lithiation increases the Nb-centred symmetry. The lithiation is probably faster at low Li^+ levels[20] owing to greater availability of sites and less interaction between cations. At lower potentials, the new EXAFS peak shifts to longer bond distances (1.85 Å) as a consequence of increased Li–O interactions at higher Li^+ content. These structural studies emphasize the value of an open, layered structure to enable rapid ion transport within the active material.

The results presented in this study establish that *T*-Nb_2O_5 exhibits electrochemical features of a pseudocapacitive material despite charge storage occurring in the bulk. Such behaviour is consistent with intercalation pseudocapacitance. The electrochemical features indicative of this mechanism are currents that are linearly proportional to the sweep rate, capacity that does not vary significantly with charging time, and peak potentials that do not shift significantly with sweep rate. A key design rule for intercalation pseudocapacitance at the atomic scale is a structure that does not undergo phase transformations on intercalation. In addition, facile two-dimensional (2D) lithium-ion diffusion pathways are

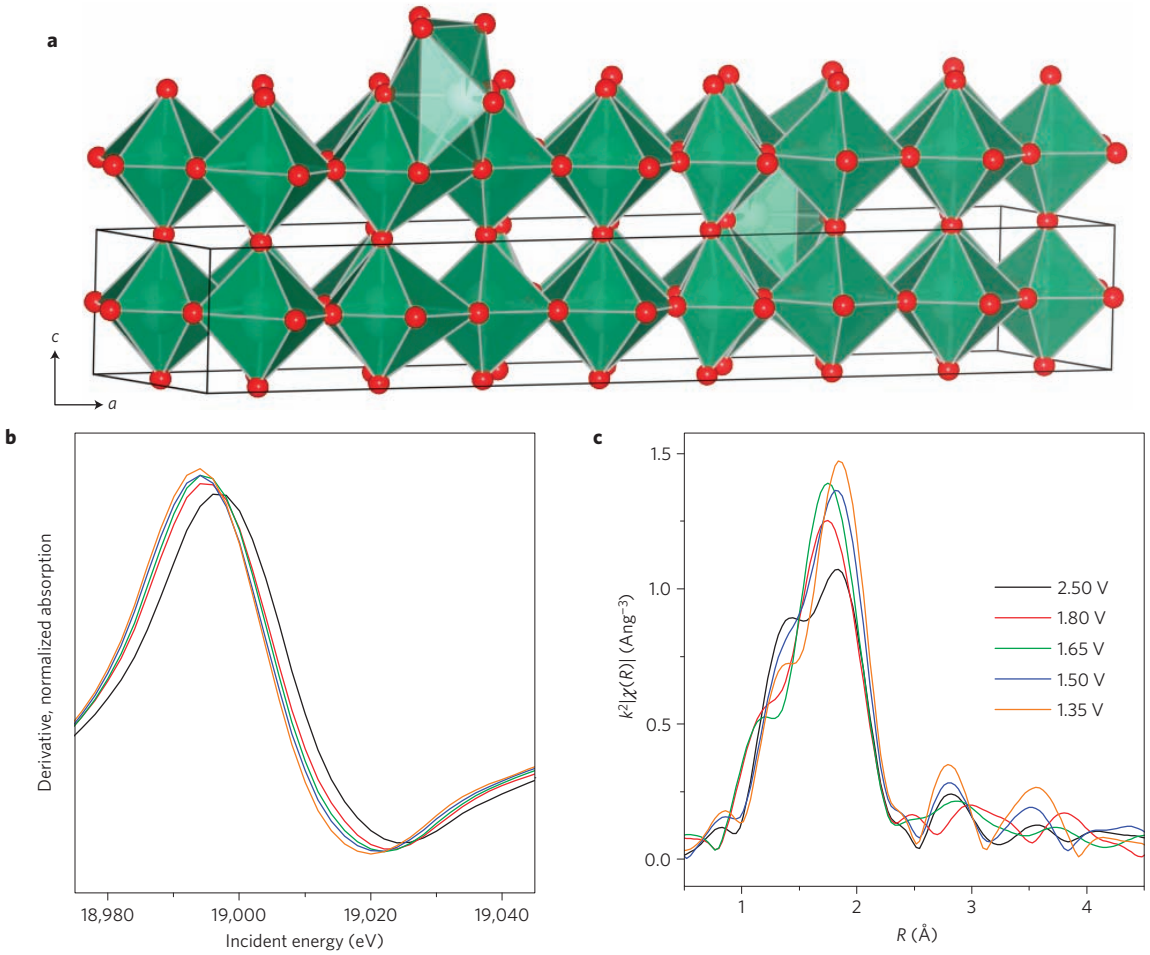

Figure 3 | Structural features of lithium intercalation in *T*-Nb_2O_5. a, The structure of *T*-Nb_2O_5 stacked along the *c* axis demonstrates the layered arrangement of oxygen (red) and niobium (inside polyhedra) atoms along the *a*–*b* plane. **b**, Derivative of Nb K-edge X-ray absorption near-edge spectra at selected cell voltages, showing a systematic shift to lower energies as Nb^{5+} is reduced to Nb^{4+}. **c**, k^2-weighted Fourier-transformed Nb K-edge EXAFS at selected cell voltages.

Table 1 | Comparison between charge storage in two different pseudocapacitive materials.

	$RuO_2 \cdot xH_2O$	*T*-Nb_2O_5
Electrolyte	H^+, aqueous[21]	Li^+, non-aqueous
Structure	Amorphous/ nanocrystalline[22,23]	Crystalline
Structural water	Necessary for proton conduction[22]	Not necessary
Charge storage mechanism	Surface/near-surface[23,24]	Bulk
Pseudocapacitance type	Surface redox	Intercalation

$RuO_2 \cdot xH_2O$ and *T*-Nb_2O_5 both exhibit capacitive behaviour. The mechanism of charge storage, however, is different and results in different structural requirements for high capacitance.

important. Charge storage that behaves as a quasi-2D process exhibits similar behaviour to 2D surface adsorption reactions[14]. These features contrast with those of pseudocapacitive $RuO_2 \cdot xH_2O$ where charge storage occurs mainly on the surface or near-surface[21–24] as summarized in Table 1.

The results here are exciting because they demonstrate that for charging times as fast as 1 min (60C rate), there are no diffusion limitations in *T*-Nb_2O_5. As the high-rate capability is due to fast ion diffusion in the bulk, this mechanism may be very good for thick electrodes because surface exposure to the electrolyte is not critical. To achieve devices with high energy density, further engineering at the nanoscale and beyond will be necessary to preserve the atomic-scale behaviour observed in thin films and microelectrodes. In particular, maintaining proper electronic conduction pathways will be critical.

Methods

Synthesis. The synthesis of *T*-Nb_2O_5 nanocrystals was reported previously[2]. Briefly, 2.56 mmol of $NbCl_5$ (Sigma-Aldrich) was dissolved in 2 ml of ethanol (Fisher Scientific). In a separate vial, 0.23 ml of deionized water was mixed with 2 ml of ethanol. Both vials were then chilled for 2 h. The two solutions were then mixed together while 1 ml of propylene oxide (Sigma-Aldrich) was slowly added, forming a transparent gel. This gel was aged for 1 day and then soaked in acetone (Fisher Scientific) for 5 days. After supercritical drying with CO_2, the gel was transformed into an amorphous Nb_2O_5 aerogel. Crystallization to the *T*-phase occurred by heat treatment at 600 °C for 2 h in air.

Characterization. Thin-film electrodes were fabricated by drop-casting a well-sonicated solution of *T*-Nb_2O_5 in ethanol onto an oxygen plasma etched stainless-steel foil (Alfa Aesar). For thin-film measurements, lithium foils (Sigma-Aldrich) served as the reference and counter electrodes, and the electrolyte was 1 M $LiClO_4$ (Sigma-Aldrich) in propylene carbonate (Sigma-Aldrich). The microelectrode preparation was described elsewhere[9]. Briefly, *T*-Nb_2O_5 active material and carbon black (Timcal Super C65) powders were mixed in a 1:1 weight ratio to ensure good electrical contact. The mixture was packed into the microcavity (30 μm depth, 30 μm width), and subsequently immersed in the electrolyte. A 1 cm^2 platinum foil (Alfa Aesar) was used as the counter electrode

and lithium foil served as the reference. Thick Nb_2O_5 electrodes were prepared by mixing the active material, carbon black (Timcal Super C65) and PVdF (Kynar) binder in a 80:10:10 weight ratio. The slurry was drop-cast onto 12-mm-diameter aluminium-disc current collectors and dried at 80 °C for 12 h. The electrode loading was between 1 and 1.5 mg cm^{-2} with a thickness of 40 ± 5 μm. Measurements of the thick Nb_2O_5 electrodes were performed in three-electrode Swagelok cells with the Nb_2O_5 electrode as the working electrode, activated carbon as the counter electrode, a glass fibre separator (Whatman, GF/A) saturated with 1 M $LiClO_4$ in propylene carbonate, and a lithium foil reference. All measurements were carried out in argon-filled glove boxes between 1.2 and 3 V (versus Li/Li$^+$) with oxygen and moisture levels of <1 ppm and using PAR EG&G 273 and Bio-Logic VMP3 potentiostats.

In situ X-ray absorption was performed using thin films of T-Nb_2O_5 cast from a well-sonicated ethanol solution onto carbon-coated aluminium. 2032-type coin cells were modified to include an X-ray window by drilling ~3-mm-diameter holes through the cathode casing and epoxying a 125-μm-thick Kapton window on the outside of the casing. Both sides of the window were then coated with 100-nm-thick aluminium layers using a vacuum evaporator. Cells were assembled with a lithium anode, a 1 M $LiClO_4$ in propylene carbonate electrolyte, and a Whatman glassy fibre separator.

References

1. Brezesinski, K. *et al.* Pseudocapacitive contributions to charge storage in highly ordered mesoporous Group V transition metal oxides with iso-oriented layered nanocrystalline domains. *J. Am. Chem. Soc.* **132,** 6982–6990 (2010).
2. Kim, J. W., Augustyn, V. & Dunn, B. The effect of crystallinity on the rapid pseudocapacitive response of Nb_2O_5. *Adv. Energy Mater.* **2,** 141–148 (2012).
3. Conway, B. E. *Electrochemical Supercapacitors: Scientific Fundamentals and Technological Applications* (Kluwer-Academic, 1999).
4. Herrero, E., Buller, L. J. & Abruña, H. D. Underpotential deposition at single crystal surfaces of Au, Pt, Ag and other materials. *Chem. Rev.* **101,** 1897–1930 (2001).
5. Huggins, R. A. Supercapacitors and electrochemical pulse sources. *Solid State Ion.* **134,** 179–195 (2000).
6. Angerstein-Kozlowska, H., Klinger, J. & Conway, B. E. Computer simulations of the kinetic behavior of surface reactions driven by a linear potential sweep. Part I: Model 1-electron reaction with a single adsorbed species. *J. Electroanal. Chem.* **75,** 45–60 (1977).
7. Brezesinski, T., Wang, J., Polleux, J., Dunn, B. & Tolbert, S. H. Templated nanocrystal-based porous TiO_2 films for next-generation electrochemical capacitors. *J. Am. Chem. Soc.* **131,** 1802–1809 (2009).
8. Lindström, H. *et al.* Li^+ insertion in TiO_2 (anatase). 2. Voltammetry on nanoporous films. *J. Phys. Chem. B* **101,** 7717–7722 (1997).
9. Come, J., Taberna, P-L., Hamelet, S., Masquelier, C. & Simon, P. Electrochemical kinetic study of $LiFePO_4$ using cavity microelectrode. *J. Electrochem. Soc.* **158,** A1090–A1093 (2011).
10. Ohzuku, T., Sawai, K. & Hirai, T. Electrochemistry of L-niobium pentoxide in a lithium/non-aqueous cell. *J. Power Sources* **19,** 287–299 (1987).
11. Park, M., Zhang, X., Chung, M., Less, G. B. & Sastry, A. M. A review of conduction phenomena in Li-ion batteries. *J. Power Sources* **195,** 7904–7929 (2010).
12. Ardizzone, S., Fregonara, G. & Trasatti, S. 'Inner' and 'outer' active surface of RuO_2 electrodes. *Electrochim. Acta* **35,** 263–267 (1990).
13. Baronetto, D., Krstajić, N. & Trasatti, S. Reply to Note on a method to interrelate inner and outer electrode areas by H. Vogt. *Electrochim. Acta* **39,** 2359–2362 (1994).
14. Conway, B. E. Transition from 'supercapacitor' to 'battery' behavior in electrochemical energy storage. *J. Electrochem. Soc.* **138,** 1539–1548 (1991).
15. Xia, H., Lu, L. & Ceder, G. Substrate effect on the microstructure and electrochemical properties of $LiCoO_2$ thin films grown by PLD. *J. Alloys Compd.* **417,** 304–310 (2006).
16. Zhang, N. Q. *et al.* Facile preparation of nanocrystalline $Li_4Ti_5O_{12}$ and its high electrochemical performance as anode material for lithium-ion batteries. *Electrochem. Commun.* **13,** 654–656 (2011).
17. Kato, K. & Tamura, S. The crystal structure of T-Nb_2O_5. *Acta Cryst.* **B31,** 673–677 (1975).
18. Liu, C-P., Zhou, F. & Ozolins, V. First principles study for lithium intercalation and diffusion behavior in orthorhombic Nb_2O_5 electrochemical supercapacitor *American Physical Society March Meeting 2012* abstr. B26.00003. Accessed March 20, 2013. http://meetings.aps.org/link/BAPS.2012.MAR.B26.3.
19. Kodama, R., Terada, Y., Nakai, I., Komaba, S. & Kumagai, N. Electrochemical and *in situ* XAFS-XRD investigation of Nb_2O_5 for rechargeable lithium batteries. *J. Electrochem. Soc.* **153,** A583–A588 (2006).
20. Kumagai, N., Koishikawa, Y., Komada, S. & Koshiba, N. Thermodynamics and kinetics of lithium intercalation into Nb_2O_5 electrodes for a 2 V rechargeable lithium battery. *J. Electrochem. Soc.* **146,** 3203–3210 (1999).
21. Long, J. W., Swider, K. E., Merzbacher, C. I. & Rolison, D. R. Voltammetric characterization of ruthenium oxide-based aerogels and other RuO_2 solids: The nature of capacitance in nanostructured materials. *Langmuir* **15,** 780–785 (1999).
22. Zheng, J. P., Cygan, P. J. & Jow, T. R. Hydrous ruthenium oxide as an electrode material for electrochemical capacitors. *J. Electrochem. Soc.* **142,** 2699–2703 (1995).
23. Dmowski, W., Egami, T., Swider-Lyons, K. E., Love, C. T. & Rolison, D. R. Local atomic structure and conduction mechanism of nanocrystalline hydrous RuO_2 from X-ray scattering. *J. Phys. Chem. B* **106,** 12677–12683 (2002).
24. Liu, Y., Zhou, F. & Ozolins, V. *Ab initio* study of the charge-storage mechanisms in RuO_2-based electrochemical ultracapacitors. *J. Phys. Chem. C* **116,** 1450–1457 (2012).

Acknowledgements

This work was supported by the Molecularly Engineered Energy Materials and the Energy Materials Center at Cornell, Energy Frontiers Research Centers funded by the US DOE Office of Basic Energy Sciences (DE-SC001342 and DE-SC0001086, respectively). XAS was performed at the Cornell High Energy Synchrotron Source, supported by the NSF and NIH/NIGMS (DMR-0936384). M.A.L. acknowledges support from the US DOD National Defense Science and Engineering Fellowship. J.C. was supported by Delegation Generale pour l'Armement (DGA). P.S. and P-L.T. acknowledge the support from the European Research Council (ERC, Advanced Grant, ERC-2011-AdG, Project 291543—IONACES) and the Chair of Excellence 'Embedded multi-functional nanomaterials' from the EADS Foundation.

Author contributions

V.A., J.C., M.A.L. and J.W.K.: experimental work, data analysis. P-L.T., S.H.T., H.D.A., P.S., B.D.: project planning, data analysis.